

Sets of Globally Optimal Stream Surfaces for Flow Visualization

M. Schulze¹ J. Martinez Esturo² T. Günther¹ C. Rössl¹ H.-P. Seidel² T. Weinkauff² H. Theisel¹

¹University of Magdeburg ²MPI for Informatics

Abstract

Stream surfaces are a well-studied and widely used tool for the visualization of 3D flow fields. Usually, stream surface seeding is carried out manually in time-consuming trial and error procedures. Only recently automatic selection methods were proposed. Local methods support the selection of a set of stream surfaces, but, contrary to global selection methods, they evaluate only the quality of the seeding lines but not the quality of the whole stream surfaces. Global methods, on the other hand, only support the selection of a single optimal stream surface until now. However, for certain flow fields a single stream surface is not sufficient to represent all flow features.

In our work, we overcome this limitation by introducing a global selection technique for a set of stream surfaces. All selected surfaces optimize global stream surface quality measures and are guaranteed to be mutually distant, such that they can convey different flow features. Our approach is an efficient extension of the most recent global selection method for single stream surfaces. We illustrate its effectiveness on a number of analytical and simulated flow fields and analyze the quality of the results in a user study.

This is the author's preprint. The definitive version is available at diglib.org and onlinelibrary.wiley.com.

1 Introduction

Flow visualization is one of the core topics in Scientific Visualization. The visual analysis of flows is especially challenging for 3D vector fields. In 3D, the *interactive* placement and integration of stream surfaces is a standard approach for exploration of the global flow behavior [ELC*12]. However, since the space of all stream surfaces is too large for systematical manual exploration [MSRT13a], the problem of *automatically* selecting suitable stream surfaces is crucial for a successful visualization. Necessary building blocks of purposeful automatic solutions to this problem are a quantifiable concept of stream surface quality and an algorithm for computing optimal solutions from the search space.

A number of methods has been proposed for computing seed curves of stream surfaces that cover the flow domain densely. All these methods evaluate *local* measures only, such as pointwise vector field quantities. Therefore, they compute locally optimal solutions in the sense that no global analysis of the search space of all possible surfaces and measurements of surface-based optimality are performed.

In contrast, Martinez Esturo et al. [MSRT13a] propose an approach to find the *globally* optimal stream surface w.r.t. new quality measures. Their approach is driven by two observations. Firstly, characteristic stream surfaces cannot be found by searching for locally optimal seed curves only: even for such seed curves the stream surface might result in a poor flow visualization when integrated away from the seed curve. Hence, finding *globally* optimal stream surfaces requires surface-based quality measures. Secondly, since opti-

mal stream surfaces are likely to occupy large portions of the flow domain and stream surfaces tend to occlude each other, it is preferable to select a *single* representative surface.

Although in many cases one single optimal stream surface gives a good representation of the flow, there are exceptions: in certain types of flow even the optimal stream surface may depict only parts of these flows, leaving other phenomena unrepresented. Examples for this are “compartment flows” with a domain divided into several different regions with low inter-region flow and distinct flow features. In such cases, an optimal *set of stream surfaces* has to be selected.

This paper solves the following problem: given a 3D steady vector field, find k stream surfaces such that they describe the vector field “best”. Here, k is assumed to be rather small, usually below ten. Martinez Esturo et al. [MSRT13a] solve this problem for the special case $k = 1$. In this paper, we present an extension and generalization to $k \geq 1$. Our goal is to find k stream surfaces such that the following conditions are satisfied: first, all selected surfaces optimize a common global quality criterion. Second, each surface should describe different aspects of the flow in a sense that they should not be mutually close to each other and avoid redundancy. The first condition is addressed in [MSRT13a] for $k = 1$. The second condition makes the selection of $k > 1$ surfaces a nontrivial problem, because generally both conditions are contradictory: if one globally optimal stream surface is found, the “next better” candidates will likely be close to this surface. This would result in a number of high quality but also very similar stream surfaces [MSRT13a].

The approach presented in this work strives towards a reasonable balance of the two conditions. It builds upon [MSRT13a] to select *one* globally optimal surface to make sure that the most prominent flow properties are captured. In fact, we follow their definition of optimal stream surfaces and the search algorithm closely. Instead of selecting stream surfaces based on a continuous priority measure, we rely on an iterative optimization for building sets of optimal stream surfaces. The basic idea is simple: in each step $1, \dots, k$ select the globally optimal stream surface, then restrict the search space for subsequent selections. A naïve implementation of this approach fails. Furthermore, the design of an efficient and practical algorithm for the selection of multiple stream surfaces based on this approach poses a number of challenges. This includes an efficient estimation of inter-surface distances, an adapted integration range of quality measures, as well as the optimization for variable integration times.

2 Related Work

This section reviews prior work including integration, rendering, and placement of stream surfaces – techniques which serve as a basis for the selection of sets of stream surfaces.

Related to the problem of stream surface placement is the placement of streamlines, which is, in general, less complex: there is a unique streamline passing through each point of the domain, whereas the number of stream surfaces passing through a point is infinite. We refer to the survey by McLoughlin et al. [MLP*10] for an overview on streamline placement methods.

Stream Surface Integration. There are many techniques addressing the practical generation of (discrete) stream surfaces. The most prominent class of methods is based on the work by Hultquist [Hul92] and uses an advancing front scheme. For an excellent overview, we refer to the survey by Edmunds et al. [ELC*12] and the references therein. More recent methods can be applied to large data sets [CGC*12] and scale integration time along the front line to obtain a near-conformal parametrization of the surface [SGRT12], which provides well-shaped elements in the discrete surface mesh.

Interactive Exploration using Stream Surfaces. Most methods rely on manual placement of seed structures to obtain stream surface geometries. Krüger et al. [KKKW05] advect stream ribbons and particles for real-time flow exploration. Martinez Esturo et al. [MSRT13b] approximate stream surfaces by flux minimization, which provides advantages for interactive exploration. There are numerous ways to improve the appearance of stream surfaces. A general goal is to ensure optimal perception of surface shape and directional information of the flow within the surface. We refer to the surveys by Laramée et al. [LvWJH04] and McLoughlin et al. [MLP*10] on visualization techniques for flow on surfaces. In recent works, Born et al. [BWF*10] enhance the visualization of stream surfaces by illustrative techniques, and Hummel et al. [HGH*10] incorporate curvature and directional information to improve perception of shape and flow. Carnecky et

al. [CFM*13] take into account findings from cognitive research to improve transparency. Günther et al. [GSM*14] use optimization to clear view on important regions of surfaces. All these methods aim exclusively at generating and visualizing stream surfaces at interactive rates. They do not address the *automatic* selection or placement of stream surfaces.

Stream Surface Placement. So far, only few methods have been proposed for automatic or semi-automatic placement of stream surfaces. Van Wijk [vW93] and Cai and Heng [CH97] use stream functions to compute sets of evenly spaced stream surfaces. Both approaches can only be applied on helicity-free flows for which a stream function integral exists.

Later, focus shifted to vector field topology: Theisel et al. [TWHS03] define and visualize saddle connectors, Weinkauff et al. [WTHS04] propose boundary switch connectors, and Peikert and Sadlo [PS09] extract topologically relevant stream surfaces. Unfortunately, these methods may extract either too many or not enough stream surfaces for representative visualizations and require the computation of vector field topology, which itself can be challenging for complex data sets.

In a recent work, Edmunds et al. [EML*12] propose the use of isolines on domain boundaries to obtain evenly spaced sets of stream surfaces by propagating seed curves into the domain. Their method requires non-vanishing flux on domain boundaries, and it strives explicitly for an even spacing of stream surfaces. In a follow-up, Edmunds et al. [ELM*12] use clustering to obtain seed curve locations to integrate sets of stream surfaces. Both approaches for seed structure selection are solely based on *local* criteria of seed curves. In particular, they do not evaluate any quality measure describing how well the selected stream surfaces represent a given flow.

Martinez Esturo et al. [MSRT13a] define such surface-based quality measures and propose an algorithm for finding a globally optimal stream surface. Their optimization method is designed to select only a *single* stream surface. It is not suited for the selection of a representative set of stream surfaces, as it would select a set of very similar and hence redundant surfaces. In this work, we overcome this limitation by extending their work: we compute sets of distinct stream surfaces that are mutually distant *and* optimal w.r.t. surface-based quality measures.

3 Background: Single Stream Surface Selection

We consider 3D steady differentiable vector fields $\mathbf{v}(\mathbf{x})$ with associated Jacobian tensor fields $\mathbf{J}(\mathbf{x})$ over flow domains \mathcal{D} . Let the *flow map* $\phi^t(\mathbf{x})$ of \mathbf{v} be the map describing the location of a particle that is seeded at \mathbf{x} after integration in \mathbf{v} for an integration time t . Then parametric *stream surfaces* \mathbf{s} are defined by parametric *seed curves* $\mathbf{c}(s)$ through integration as $\mathbf{s}(s, t) = \phi^t(\mathbf{c}(s))$.

In this paper, we extend the stream surface selection method by Martinez Esturo et al. [MSRT13a] to the global selection of sets of characteristic stream surfaces. In this section, we briefly review the essentials of their approach before describing our extensions.

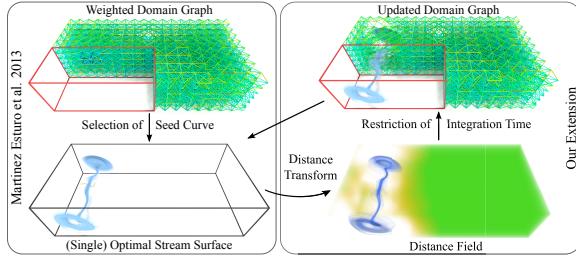


Figure 1: Algorithm Overview. We extend the single stream surface optimization method [MSRT13a] (left) to the selection of multiple surfaces (right) by employing the selection algorithm on an updated weighted domain graph (• cutaway regions). Edge cost updates are based on restriction of ribbon integration times by inter-surface distance enforcement. Our selected set of stream surfaces for this BÉNARD compartment flow example is shown in Figure 7.

The original method is designed to select a single stream surface that optimizes a set of quality measures. The quality measures are evaluated on narrow stream ribbons that are integrated from edges of a spatial graph that covers the domain densely. This way, costs are assigned to each graph edge. Then, a global optimization is performed for the path of minimal costs and a given number of edges, which determines the seed curve of the selected globally optimal stream surface.

Quality Measures. The quality measures of [MSRT13a] are designed to prefer characteristic stream surfaces. They are defined generically by integrated intrinsic surface properties, i.e., they are application-independent as they are neither specialized nor restricted to a specific flow feature type.

The first quality measure considers the alignment of the flow in the surface with principal curvature directions of the surface. It describes the local variation of normal curvature in flow direction and is therefore a measure of surface fairness. Additionally, this measure has a perceptual interpretation in that it measures how well flow is perceivable on the stream surface. Formally, the *local alignment error* reads as $e_a = \mathbf{n}^T \mathbf{J}(\mathbf{v} \times \mathbf{n}) / \|\mathbf{v}\|^2$ and depends on both local flow properties and the surface orientation given by the surface normal direction \mathbf{n} . For optimization, the *average squared alignment error* is considered by integrating e_a^2 over a stream surface $\mathbf{s}(s, t)$ with full parametrization $(s, t) \in [s_0, s_1] \times [t_0, t_1]$:

$$E_a = \frac{1}{A} \int_{t_0}^{t_1} \int_{s_0}^{s_1} e_a^2 \|\mathbf{s}_s \times \mathbf{s}_t\| \, ds \, dt. \quad (1)$$

Here, $\mathbf{s}_s = \frac{\partial}{\partial s} \mathbf{s}$ and $\mathbf{s}_t = \frac{\partial}{\partial t} \mathbf{s}$ denote the partial derivatives of the surface with area A . This averaged error is comparable for stream surfaces of different area.

The alignment error E_a is the primary optimization target. However, it has trivial minimizers in form of planar surfaces. To penalize trivial solutions, the second quality measure considers the *normal curvature* $\kappa_n = \mathbf{n}^T \mathbf{J} \mathbf{v} / \|\mathbf{v}\|^2$ of a stream surface in flow direction. It is used to compute the *average squared normal curvature*

$$K_n = \frac{1}{A} \int_{t_0}^{t_1} \int_{s_0}^{s_1} \kappa_n^2 \|\mathbf{s}_s \times \mathbf{s}_t\| \, ds \, dt, \quad (2)$$

which is generally maximized.

A third quality measure E_p penalizes seed curves that are aligned tangentially to the flow and would lead to degenerate stream surfaces. Finally, the selection method tries to maximize stream surface area A as a fourth quality measure.

Surface Selection. The algorithm in [MSRT13a] minimizes these quality measures in order to automatically select a single, globally optimal stream surface. An overview of this algorithm is shown in Figure 1 (left). The basic idea of the selection method is to find the optimal stream surface by constructing its seed curve out of optimal small curve segments. The search space of seed curves is discretized using a domain-spanning weighted graph (Figure 1 (top left)). Each edge has an associated non-negative edge cost. Edge costs are computed by evaluating the quality measures on narrow stream ribbons that are integrated from each edge, i.e., they are a weighted combination of terms considering E_a , K_n , E_p , and A . The full domain integration by stream ribbons from each edge is the costliest step, but it is mandatory for a global optimization. Simple paths in this graph then serve as candidate seed curves of larger stream surfaces that can be considered as the union of all stream ribbons seeded at the edges of the path. Stream surface quality can then efficiently be evaluated by the sum of costs of each edge of the path. A global *Simulated Annealing* (SA) optimization [KGV83] is performed that improves candidate paths until the globally optimal path of minimal costs is found. The final optimal stream surface \mathbf{s}^* is obtained by integrating from the selected path, which is smoothed to a continuous curve prior to integration. Figure 1 (bottom left) shows an exemplary result.

For a detailed explanation of the method we refer to the original work by Martinez Esturo et al. [MSRT13a]. Now, we start to construct an algorithm for the selection of a set of optimal and non-redundant stream surfaces.

4 Selection of Sets of Stream Surfaces

Flow data sets may contain only a single dominant global feature. In these cases, the selection of a single globally optimal stream surface is sufficient to represent and visualize the flow [MSRT13a]. However, this assumption does not hold for flow containing more than a single global feature: flows with separate closed flow compartments are examples for this type of data sets that cannot sufficiently be represented by a single stream surface. Figure 1 exemplifies this for the BÉNARD flow. Such flows require the selection of a set of characteristic stream surfaces (cf. our BÉNARD result in Figure 7).

In the following, we extend the global stream surface selection method by Martinez Esturo et al. [MSRT13a] towards the selection of a set $\mathcal{S}_k = \{\mathbf{s}_1^*, \dots, \mathbf{s}_k^*\}$ of $k \geq 1$ optimal stream surfaces. Our approach is iterative, and in each iteration a set \mathcal{S}_k is extended by the *optimal* surface in the search space that is restricted by the surfaces in \mathcal{S}_k to give the next set \mathcal{S}_{k+1} .

To achieve this, we introduce an efficient edge cost update scheme, which is performed in every iteration. For efficiency,

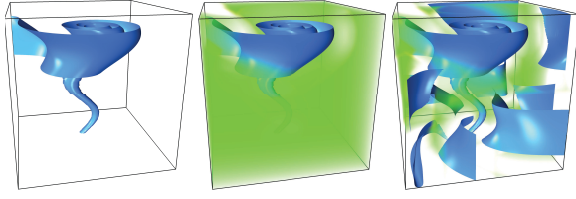


Figure 2: Inter-Surface Distance Field. For the globally optimal stream surface initially selected by [MSRT13a] in the TORNADO flow (left) we compute a distance field using Euclidean Distance Transform (• volume rendering, $d_{\min} = 8l/100$) (center). It is used to restrict the search space for further selected stream surfaces (right). The distance field is updated for each selected surface.

iterations reuse as much data as possible from the single surface selection method. In particular, we show that a single initial domain integration is sufficient to select even a set of optimal stream surfaces. Ideally, each stream surface of this set optimizes the same quality criteria in the subspace restricted by the other surfaces, and surfaces should be distinct and mutually distant for non-redundant domain sampling.

For surface optimization, this requires efficient evaluation of integration-time restricted quality measures and inter-surface distance computations. Figure 1 (left) illustrates the main steps of our extension. We continue to provide details.

4.1 Inter-Surface Distance Estimation

We demand that the stream surfaces \mathbf{s}_i^* describe different flow characteristics and avoid redundancy. This implies that surfaces are mutually different in a sense that they should not get close to each other. Formally, this means that some *lower bound* for inter-surface distance is maintained. This condition is similar but not equivalent to selection methods for streamlines [JL97] and surfaces [vW93, CH97, EML*12], as these methods aim for lines and surfaces that cover the domain evenly. Compared to these approaches, our lower bound condition is less restrictive and can yield evenly placed surfaces as a special case.

We prescribe a lower bound d_{\min} for all pairwise inter-surface distances and compute an efficient approximation of a distance field $d(\mathbf{x})$ to all selected surfaces using a *Euclidean distance transform* (DT) proposed by Saito and Toriwaki [ST94]. This is a well-known technique, e.g., in Computer Vision or Geometry Processing [FCTB08]. The domain is first partitioned by a regular grid. Then the distance field is constructed such that each voxel is assigned the distance to a zero contour given as “obstacle voxels”. In our case, obstacle voxels are determined by rasterization of the current set of selected stream surfaces such that each voxel intersected by a stream surface mesh is marked as an obstacle. The distance field is then used to decide whether a particular candidate surface point is valid w.r.t. the distance threshold d_{\min} . The run-time of the DT method is independent of the number of surfaces and scales well even for high voxel resolutions. In practice, we specify the threshold d_{\min} relatively to the

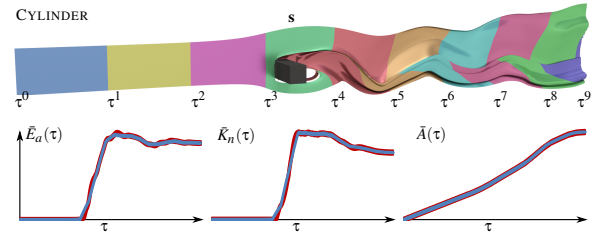


Figure 3: Quality Measure Segmentation. Stream surfaces \mathbf{s} are partitioned into equidistant segments $[\tau^i, \tau^{i+1}]$ along integration time for efficient measure evaluation (top). Our piecewise linear approximation of surface-integrated quality measures on this segmentation (thin •) is close to the exact integration (•), as shown in the graphs (bottom) for the measures $\bar{E}_a(\tau) \equiv \bar{E}_a(\tau_0, \tau)$, $\bar{K}_n(\tau) \equiv \bar{K}_n(\tau_0, \tau)$, and $\bar{A}(\tau) \equiv \bar{A}(\tau_0, \tau)$ on the benchmark surface \mathbf{s} .

length l of the domain bounding box diagonal. Its value steers surface density, and we demonstrate the effect of varying d_{\min} in Section 5.2. In all experiments we use a regular grid with approximately cubic voxels for the representation of $d(\mathbf{x})$ with a resolution of 100 voxels for the dimension with the longest domain extent. Exemplary distance fields visualized by volume rendering are shown in Figure 2.

While it is possible to discard every stream surface candidate that falls below d_{\min} for any point on the surface, we propose an alternative and more accurate approach that is based on restriction of integration time. This way only parts of surfaces will be discarded.

4.2 Integration Time-Restricted Quality Measures

For the selection of multiple stream surfaces, we require the range of integration times as an additional optimization target. We extend the quality measures of [MSRT13a] (see Section 3) such that a restriction of integration times is incorporated in an efficient manner. This way, all of our selected surfaces share the same global quality criteria in their restricted search spaces. This will also guarantee us to select the same globally optimal surface \mathbf{s}_i^* among the set of selected surfaces.

Given a surface-integrated quality measure we define an integration time-restricted version by restricting the full time range $[t_0, t_1]$ to $[\tau_0, \tau_1]$ with $t_0 \leq \tau_0$, $\tau_1 \leq t_1$, i.e., only a smaller surface part centered around the seed curve is considered. For instance, the average squared flow alignment measure E_a in (1) becomes

$$\bar{E}_a(\tau_0, \tau_1) = \frac{1}{\bar{A}(\tau_0, \tau_1)} \int_{\tau_0}^{\tau_1} \int_{s_0}^{s_1} e_a^2 \|\mathbf{s}_s \times \mathbf{s}_r\| \, ds \, d\tau \quad (3)$$

with the restricted surface area $\bar{A}(\tau_0, \tau_1) = \int_{\tau_0}^{\tau_1} \int_{s_0}^{s_1} \|\mathbf{s}_s \times \mathbf{s}_r\| \, ds \, d\tau$. The restricted average squared normal curvature $\bar{K}_n(\tau_0, \tau_1)$ (see (2)) is defined similarly. The estimation of the restricted time range $[\tau_0, \tau_1]$ will be discussed in Section 4.3.

Note that a restriction of the seed curve range $[s_0, s_1]$ is not required. This can always be achieved by changing the path length and possibly increasing the domain graph resolution.

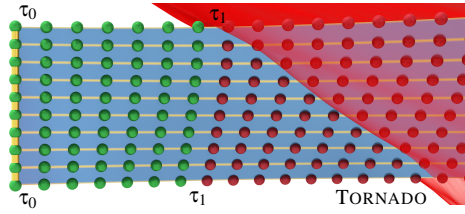


Figure 4: Estimation of Integration Times. For each graph edge a set of streamlines (●) is integrated that evaluate the distance field (● isocontour $d(\mathbf{x}) = d_{\min} = l/10$) for the restricted integration time range $[\tau_0, \tau_1]$ of the stream ribbon (●). τ_1 is the maximal integration time for which all streamlines at least d_{\min} -distant to any other surface (●).

Quality Measure Discretization. For optimization, time-restricted quality measures need to be evaluated for different $[\tau_0, \tau_1]$ values several times. The exact evaluation of the integrals turns out to be prohibitively expensive as all stream ribbon surfaces would need to be kept in main memory (see Section 5.4). Instead, we approximate restricted quality measures in a piecewise (and memory-efficient) way by exploiting additivity of integrals: we first partition a triangulated stream surface into equidistant segments $[\tau^i, \tau^{i+1}]$ along integration time. The integrated measure value is computed for each segment by a single point quadrature at each triangle center and saved for each surface segment (see Figure 3 (top)). For measure evaluation, we determine all segments that are completely contained in the requested time range $[\tau_0, \tau_1]$ and add their associated integrated value to the result. For partially covered segments only the fractional part is added. This discretization yields piecewise linear approximations of the exact integrals \bar{E}_a , \bar{K}_n , and \bar{A} similar to (3). We compare this approximation to the exact integrals for a stream surface in the CYLINDER flow in Figure 3 (bottom). Even for this bifurcating surface our approximation is sufficiently close to the original integrals as approximation errors do not accumulate. Note that contrary to this example, for optimization the restricted measures are generally only evaluated on narrow stream ribbons that are integrated from graph edges. Using a fixed number of 25 segments has shown to be sufficient in all our experiments.

4.3 Integration-based Distance Sampling

To evaluate time-restricted quality measures the restricted time ranges $[\tau_0, \tau_1]$ need to be estimated for each graph edge. For a given stream ribbon, they describe the part of the surface that has a distance of at least d_{\min} to all other currently selected stream surfaces. Assuming forward integration only this corresponds to the problem of determining the longest forward integration time $\tau_1 \leq t_1$ for which $d(\mathbf{x}) > d_{\min}$ holds for all stream ribbon points \mathbf{x} (and similarly $t_0 \leq \tau_0$ for backward integration).

A straightforward way to estimate τ_1 is to evaluate $d(\mathbf{x})$ on each vertex \mathbf{x} of the stream ribbon. However, even for coarsely tessellated stream ribbons, this results in a large number of distance field evaluation points that possibly exceed memory

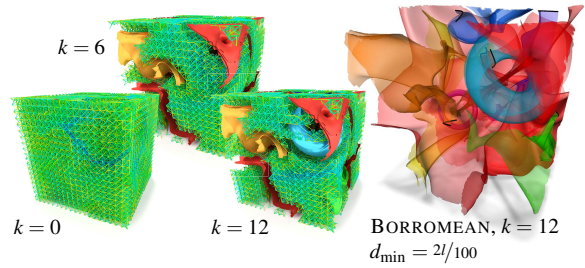


Figure 5: Iterative Edge Costs Update. Left: the domain graph with per-edge graph costs (low ●, high ●) at different iterations k combined with the currently selected surfaces. Right: the final set of stream surfaces \mathcal{S}_{12} . In each iteration, edge costs are updated by the evaluation of quality measures on integration time-restricted stream ribbons.

restrictions for complex flow fields (see the discussion on memory footprints in Section 5.4).

Instead, we propose an approximate but more efficient approach that has shown to be sufficient in all our experiments: we use a representation on a fixed size parametric grid and sample each surface ribbon along iso-parametric $s = \text{const}$ surface curves. Algorithmically, this means for each edge we integrate a fixed number of equidistant streamlines and save them for further distance sampling. To estimate the new restricted integration time τ_1 , we evaluate $d(\mathbf{x})$ on each streamline vertex \mathbf{x} . Figure 4 illustrates this approach: valid streamline vertices in the integration time range $[\tau_0, \tau_1]$ are marked (●) whereas invalid vertices are colored (●). Our experience is that the evaluation of ten streamlines per edge approximate the stream ribbons very well as they are narrow in general. Note that the additional costs for integration of these streamlines for each edge are negligible as they can be computed in parallel along with the initial domain-wide per edge stream ribbon integration.

4.4 Sets of Optimal Stream Surfaces

The sets of stream surfaces are selected iteratively, and in each iteration the set of stream surfaces \mathcal{S}_k is extended by the current globally optimal stream surface \bar{s}^* in the search space restricted by \mathcal{S}_k . Figure 1 (right) illustrates the optimization while an exemplary iteration is shown in Figure 5. We compute \bar{s}^* in the following way by applying the proposed building blocks of this section: in each iteration, the distance field $d(\mathbf{x})$ is updated for all surfaces in \mathcal{S}_k (see Section 4.1). Then we restrict the search space of feasible stream surfaces by computing new per-edge integration times $[\tau_0, \tau_1]$ of each stream ribbon relative to $d(\mathbf{x})$ and the prescribed minimal inter-surface distance d_{\min} (see Section 4.3). Stream ribbon integration time restriction yields reduced integrated quality measures \bar{E}_a , \bar{K}_n , and \bar{A} at each edge, which are evaluated using the memory-friendly approximation of Section 4.2. (Note that the flow orthogonality term E_p of each edge is unchanged as it is no surface-integrated measure). Graph edges for which the resulting restricted total ribbon area \bar{A} vanishes are removed. From hereon we continue to perform

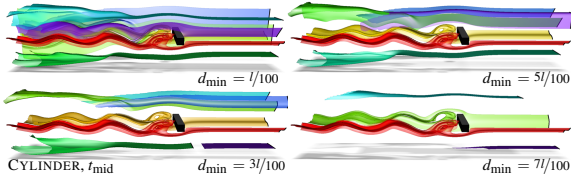


Figure 6: Surface Density Variation. Increasing the minimal inter-surface distance d_{\min} yields stream surface sets of lower density. Note that the first selected stream surface (\bullet) is always equal, whereas the seed curves and integration times of subsequent surfaces vary for different d_{\min} values.

a surface selection as described in [MSRT13a]: the reduced quality measures are used to compute new edge costs of the graph, a global simulated annealing-based optimization selects the optimal simple path of minimal costs in the updated graph, and a smoothed seed curve \bar{c}^* is generated from the optimized path by a corner cutting scheme [Sab10]. Then \bar{s}^* is integrated from \bar{c}^* by respecting the restricted integration times $[\tau_0, \tau_1]$ of each edge of the path. For this, we extended the stream surface integration method by Hultquist [Hul92] to support varying integration times along the seed curve. Finally, \bar{s}^* is added to \mathcal{S}_k and this procedure is iterated until a prescribed number k of stream surfaces has been selected or no more surfaces can be selected for the specified d_{\min} .

5 Results

In this section, we present results for selecting stream surface sets for different vector fields types. We start with a brief review of the visualization and a discussion of the parameters of our approach, and we conclude the section with timings.

5.1 Visualization

We visualize stream surfaces using the IRIS approach by Hummel et al. [HGH*10], who use viewing angle-dependent opacity for well-perceivable semi-transparent stream surface renderings to minimize occlusion problems. The color of stream surfaces indicates the selection order as depicted at the bottom of Figure 7. The (\bullet) surface is always the stream surface that is selected first, i.e., it coincides with the single surface selected by [MSRT13a].

5.2 Parameters

Our method inherits the parameters from the single surface selection method [MSRT13a] and *only* introduces two additional intuitive parameters: the number of surfaces k and the minimum distance threshold d_{\min} . The inherited parameters are the target mean normal curvature, the domain graph resolution, and the path length and path curvature factor. Unless noted otherwise, in all experiments we use the default values suggested by the authors of the original method and refer to their work for a description of these parameters.

Our approach selects a set of stream surfaces based on the minimal inter-surface distance parameter d_{\min} . Its value is inversely proportional to the density of the selected surfaces, i.e., increasing minimal distances results in decreasing

surface density. We show an example of this relation in the CYLINDER flow in Figure 6. Our experiments show that reasonable choices for a variety of data sets are $d_{\min} \in [l/100, l/5]$, where l denotes the length of the domain bounding box diagonal. Also, the efficiency of our multiple surface selection extension (see Section 5.4) allows to fine-tune this value if required once the domain integration has been performed. Still, the optimal d_{\min} value certainly depends on feature size and reflects the desired surface proximity.

Suitable values for the number k of stream surfaces strongly depend on the flow characteristics, most importantly on the number of features and feature distribution. As multiple features can be represented well by a single stream surface [MSRT13a], the required number of stream surfaces is not known a priori. Still, in all our experiments the number k of required stream surfaces tends to be rather low: we use at most $k = 12$. More importantly, our user study (see Section 6) shows that it is easy for flow visualization experts to choose k values for representative flow visualizations. As the computational costs for additional surfaces are also low (see Section 5.4), we use the following approach: we compute and present the user a series of — usually ten — surfaces, which she then can explore interactively for different values of k . This includes the extension of the set of surfaces as on-demand computations of additional surfaces works at interactive rates. A feasible alternative is to stop extending the set once a new surface falls below a minimal area threshold.

5.3 Results: Selected Sets of Stream Surfaces

In the following, we present results for both, analytical and simulated vector fields. In addition, we would like to refer to the **accompanying video** for illustrations of the optimization algorithm and more extensive visualizations of the results.

Analytical Vector Fields. Simple linear and analytical vector fields usually do not contain a high number of distinct features and multiple stream surfaces are not mandatory for their visualization. Still, they are well-suited to illustrate different properties of our approach, and we show three examples in Figure 7 (left): the TORNADO flow consists of a single vortical structure [GRT13] that is represented well by the globally optimal stream surface [MSRT13a: Fig. 5]. Additional surfaces do not contribute to the representation of the feature (cf. Edmunds et al. [EML*12: Fig. 7]). Rather, they only provide additional context information near the dominant structure, and in this case distance enforcement leads to a spatially even distribution of additional surfaces. For the well-known linear SPIRAL flow we show results that either maximize or minimize the squared mean normal curvature K_n in (2) (we maximize K_n in all other examples of this work). Our distance-aware extension of the global quality measure optimization yields symmetric results in both cases. In addition, we use the simple TWOFOCI flow, which has a dominant planar separating structure between two focus points, as a test data set in the user study (see Section 6 and the additional material). Again, our method selects a symmetric result.

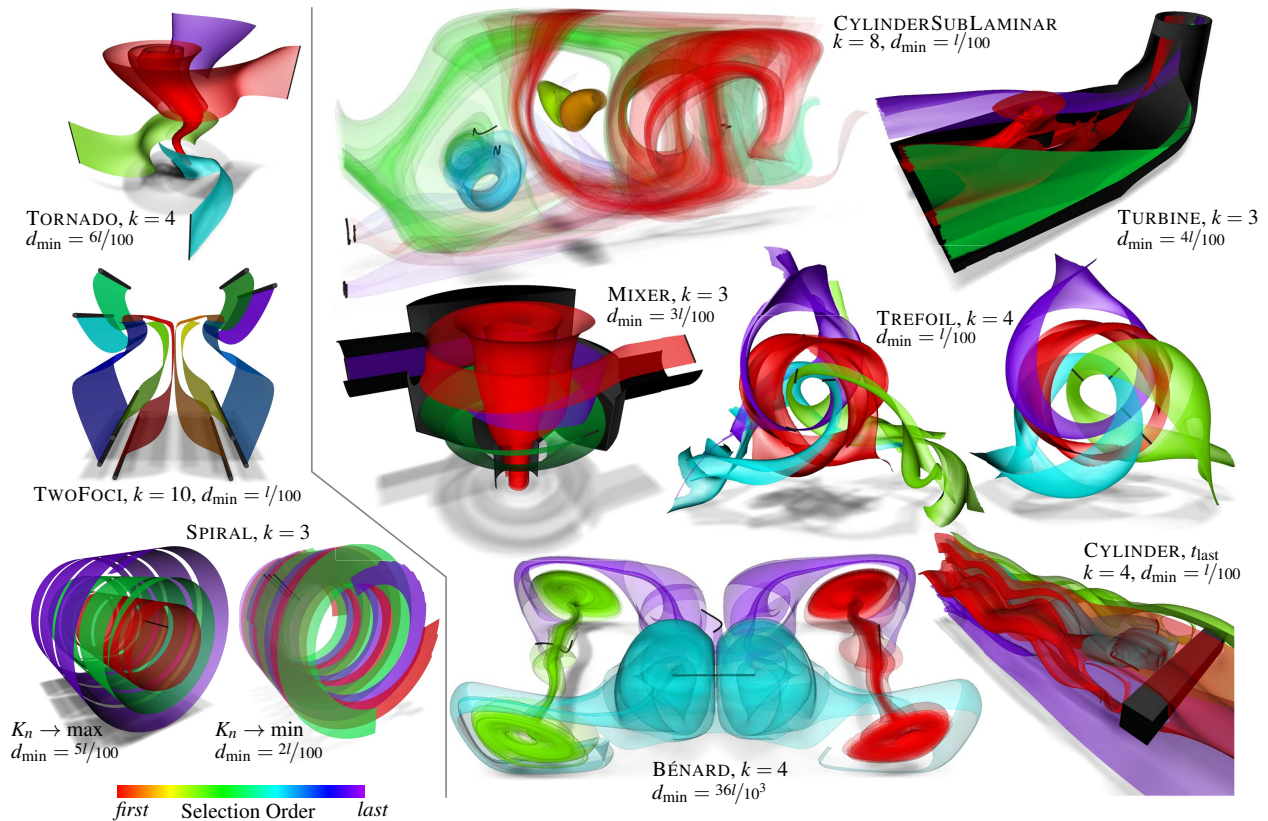


Figure 7: Selection Results for Analytical and Simulated Vector Fields. Left: analytical fields are suitable to illustrate properties of our method: selected sets of stream surface respect the minimal distance bound and represent the major flow features. Surface color encodes selection order (bottom left), seed curves are colored (●). All examples maximize the squared mean normal curvature K_n and we also show its minimization for the SPIRAL flow. Right: for simulated fields of varying characteristics we show the selected stream surface sets S_k . Two time steps of a magnetic flux decay simulation are shown for the TREFOIL flow.

Simulated Vector Fields. More complex simulated flows usually contain multiple flow features or can be segmented into multiple disjoint compartment regions. Therefore, these flows are likely to require multiple stream surfaces for the uniform representation of the whole flow domain. We present automatically selected stream surface sets in this type of flows in Figure 7 (right). Based on the well-known flow behind a cubic CYLINDER (cf. Edmunds et al. [ELM*12; Fig. 14], also shown in Figure 6 for an earlier time step, see also [CSBI05, BFTW09, ELM*12, EML*12, SGRT12, MSRT13a]) the CYLINDER_{SUBLAMINAR} data set is obtained by removing the laminar flow component. This flow is used to study the extraction and tracking of multiple vortex core lines [SWH05, TSW*05]. Our method selects a set of stream surfaces that contains both surfaces that are close to these core lines and surfaces that represent the vortical flow context. A single stream surface is not sufficient to visualize all features of the data set and our method captures more features with uniformly distributed stream surfaces.

The Rayleigh-BÉNARD flow is an example with separate compartments, which is a simulated data set of fluid motion as the result of thermal convection (cf. Edmunds et al. [ELM*12;

Fig. 15]) [WSE05, GRT13]. Again, a single globally selected stream surface can only partially represent the data set (see Figure 1). Using only four stream surfaces our method detects a symmetric result in which two outmost vortical flow compartments are connected symmetrically by two center flow regions.

The simulation of the outlet area of a hydroelectric turbine that comprises a flow bifurcation is analyzed in the TURBINE data set [SGRT12, MSRT13a, MSRT13b]. The initial stream surface captures both dominant features: the bifurcation and the only vortical flow structure near the split region — in this case further surfaces provide a visualization of the remaining laminar flow context.

The efficiency of a radial fluid mixing device with two inlets and one outlet at the bottom is studied in the MIXER flow. Only after the selection of three surfaces all openings and the main vortical structure in the center are captured by the set of stream surfaces.

The simulated TREFOIL field represents the time-dependent field lines of interlocked magnetic flux tubes and is used to study magnetic energy decay processes like coronal mass ejections of the sun [CDSB11]. The initial configuration

Data set (k)	EDGES ($\cdot 10^9$)	MEMORY (GB)		COMPUTATION TIME (s)					
		QM	SL	I	DT/it	EC/it	SA/it	T(1)	T(k)
BÉNARD (4)	23.0	0.09	1.7	171.9	0.37	1.09	1.8	175.8	185.1
BORROMEAN (6)	35.2	0.14	2.3	283.7	0.47	2.62	2.5	290.0	319.2
CYLINDER (6)	8.1	0.04	1.1	134.3	0.35	0.96	1.1	137.6	149.1
CYLINDERSUBL. (8)	28.1	0.10	2.0	225.3	0.44	2.04	1.9	230.1	263.8
SPIRAL (4)	3.2	0.01	0.3	15.2	0.32	0.23	0.8	16.8	21.4
TWOFOCI (10)	4.1	0.02	0.6	17.3	0.35	0.30	0.8	17.1	23.0
TORNADO (4)	7.3	0.02	1.0	20.3	0.38	0.45	1.1	22.7	29.0
TREFOIL (4)	14.3	0.05	1.3	145.3	0.36	1.09	1.3	148.1	156.3
MIXER (3)	7.8	0.03	1.1	22.7	0.36	0.51	1.1	24.9	31.1
TURBINE (4)	8.8	0.05	1.3	82.7	0.35	1.05	1.2	85.5	93.9

Table 1: Memory Footprints and Timings. For each data set we show the total number of graph edges, the memory consumptions of the discretized surface-integrated quality measures (**QM**) and streamlines (**SL**), as well as computation times of each phase of our approach: ribbon/streamlines integration (**I**), distance transform per iteration **DT/it**, edge costs update per iteration **EC/it**, simulated annealing optimization per iteration **SA/it**, and the total computation time $T(k)$ for k surfaces. Only the columns with bold titles are needed to compute additional surfaces.

is a trefoil knot of flux tubes and the two analyzed time steps show an early and a progressed decayed state. In both time steps, our method faithfully extracts the three symmetrically arranged decayed rings together with a centered closed stream surface representing the mean magnetic field of the surrounding rings. A related experiment for three interlocked magnetic BORROMEAN flux rings [CB11] is shown in Figure 5.

Our results show that the single globally optimal stream surface (•) often represents the whole flow domain only partially. Hence, the visualization of sets of stream surfaces is preferable if the flow data contains multiple features or is subdivided into compartments. The preference of multiple, non-redundant stream surfaces is also backed by the comparatively low additional computational costs, which are required for the selection of additional surfaces. We analyze the performance of our method in the following section.

5.4 Timings

We measured both, memory requirements and execution times of each phase of our approach on a Linux PC equipped with an Intel Core i7-4770K 3.5GHz quad core CPU and 16GB main memory. For the data sets used in this work we summarize the resulting values together with the number of graph edges in Table 1. Flow data sets are discretized on regular grids and resolutions range from 50^3 cells for the SPIRAL flow to 256^3 cells for the BORROMEAN flow. Note that in each iteration we only require the fields typeset **bold** to extend the set of stream surfaces by an additional surface. Similar to the single surface selection method, we run the most time-consuming step of global ribbon and streamline integration (**I**) in parallel on multiple CPU cores [MSRT13a]. This step results in a *significant* amount of ribbon mesh data (up to 31.2GB for the BÉNARD flow), which we can *effectively* reduce for multiple stream surface selection by up to 92% using the proposed quality measure approximation

(**QM**) and streamline-based distance estimation (**SL**). Similar to [MSRT13a], total execution times $T(k)$ indicate that our automatic selection method is an offline analysis process and provides no instantaneous results. Still, once the full domain integration is performed, our proposed method for the selection of *additional* surfaces turns out to be very efficient: the distance field update **DT**, edge cost update with restricted integration time estimation **EC** as well as the simulated annealing-based minimal path optimization **SA** that are performed in each iteration are computed at interactive rates. Hence, by reusing data from the full domain integration, our multiple surfaces selection times $T(k)$ are very low compared to single surface selections $T(1)$. Note that the **DT** execution time is proportional to distance field resolution and independent of the number of surfaces, and its memory requirements are constant. Moreover, as we represent the surface-integrated quality measures in a very compact form that does not require vector field sampling for evaluation anymore, edge cost updates are cheaper to compute compared to an initial full evaluation [MSRT13a].

6 User Study

To evaluate the effectiveness of our method, we conducted a user study with 22 participants consisting of CFD experts and users with a strong visualization background. We compare two competing stream surface selection techniques: classical stream surface selection where users place surfaces manually, and our automatically selected sets where users select suitable values for the number k of surfaces. Participants use both techniques to create visualizations for analytical (TWOFOCI and TORNADO) and more complex simulated (BÉNARD and TREFOIL) flows, which are then assessed in terms of how representative is the visualization, degree of satisfaction, and ease of use by the users. In summary, the majority of participants agrees that their visualizations using our automatically selected stream surfaces are representative for the tested data sets and that they are satisfied with the results. Visualization representativeness, user satisfaction, and ease of use using our approach is higher compared to manual selection while the required active interaction time is significantly lower for our method (excluding the unsupervised preprocessing time). The additional material includes a more detailed **study description** and **evaluation**, and a **video** of typical participant interactions.

7 Discussion

Feature extraction generally focuses on a single well-defined type of flow structure, whereas stream surfaces are applied in a more general way to convey global flow behavior. These different visualization goals make both methods orthogonal to each other. Still, we observe a relationship: even though there is no guarantee that all flow features are represented by our sets of stream surfaces, it is often possible to deduce the presence of features from the selected surfaces. For instance, compare our result for the BOR-

ROMEAN rings flow shown in Figure 5 (right) with explicitly extracted distinct characteristic features (see inset): closed streamlines (●) representing the ring structures and the dominant diagonal vortex core line (●, extracted by [SH95]). In this particular example, torus-like rings are selected due to their vanishing normal curvature variation with simultaneous non-vanishing normal curvature. Note that this argument also holds for other selections, such as the cylindrical structure around the central vortex core line.



The method by Edmunds et al. [ELM*12] shares our goal to automate the task of stream surface selection. We provide results on identical data sets in Figure 7 for the BÉNARD and CYLINDER flows. Both methods share several properties: the algorithms require no feature extraction and use a uniform space discretization to search for flow-orthogonal seed curves. Our seed curves are as-orthogonal-as-possible to the flow whereas the seed curves in [ELM*12] are flow-orthogonal by construction. While our method performs a domain-wide stream surface integration to evaluate surface-based quality measures, their method uses hierarchical vector field clustering based on pointwise field properties, such as magnitude and curvature. This makes their method perform faster and independent of shape and integration time of the resulting stream surfaces. While our approach allows to preserve mutual distance of the selection stream surfaces in order to reduce visual clutter, the local, pointwise approach in [ELM*12] does not take this into account.

Referring to the single stream surface selection method by Martínez Esturo et al. [MSRT13a] that considers surface-based quality measures, we emphasize that we generalize their approach towards surface sets. As our discretization of integration time-restricted quality measures accurately interpolates the exact surface integrals of [MSRT13a] (see Section 4.2), we are *guaranteed* to reproduce their single globally optimal stream surface (see, e.g., the CYLINDER, TORNADO, or SPIRAL flows in [MSRT13a: Fig. 5]). This way, surfaces of the automatically selected sets inherit the important property of being very similar to stream surfaces that have been *manually* selected by domain experts (see also the discussion in [MSRT13a]). In addition, our user study shows that CFD and visualization experts rate our selection results to be *representative* for the tested data sets.

Our method uses a *greedy* selection of stream surfaces: every surface is globally optimal w.r.t. the *current* search space, which in turn is determined by restricting distance to all previously selected surfaces. The convergence of the SA optimization to globally optimal solutions in a given search space is stated in [MSRT13a]. Our results indicate that this greedy approach is effective for a variety of different flow data sets. Still, we cannot guarantee that the selected sets S_k minimize the *accumulated* quality measures over all possible sets of k surfaces. This would require an approach that *simultaneously* optimizes for multiple surfaces minimizing surface-based quality measures and respecting their inter-surface distances, which is a far more complex problem. We emphasize that

such a simultaneous global optimization does not even exist for the simpler problem of streamline placement [MLP*10]. Moreover, greedy algorithms are successfully applied in computer graphics and visualization. For instance, mesh simplification algorithms similarly minimize global measures using a greedy strategy: the result may be a local minimum, but is accepted as close to optimal.

The presented results indicate that our method yields convincing visualizations for a series of different flow phenomena. Yet, we note that surface-based visualizations in general are of limited use for highly turbulent flows, which is also a limitation of our method. Additionally, even a single opaque stream surface can occasionally exhibit a high amount of occlusion, which can be regarded as a limitation of *any* stream surface selection method. Still, we argue that stream surface selection and rendering are related but different problems: we have shown that for a variety of data sets a single stream surface does not suffice in representing all flow features, and multiple, but potentially occluding, surfaces are required for a complete representation of the characteristic features of the flow domain. Whereas we use the IRIS rendering approach by Hummel et al. [HGH*10] to minimize occlusion, the more recent method by Günther et al. [GSM*14] is an even more advanced approach for minimization of surface occlusion.

8 Conclusions

In this work, we present a method for the automatic selection of a set of stream surfaces for which all its surfaces optimize a global quality criterion. This is in contrast to other selection approaches that do not evaluate the quality of stream surfaces or are limited to the selection of a single stream surface. Alongside the minimization of stream surface quality measures our method also considers inter-surface distances and selects non-redundant stream surfaces that respect a minimal inter-surface distance bound. We demonstrate the requirement of sets of stream surfaces and the effectiveness of our method for a number of different analytical and simulated data sets. In a user study with 22 participants, the majority agrees that our visualizations are representative for the tested data sets and that they are satisfied with the results.

The automatic selection of time-dependent streak and time surfaces is an unsolved problem of major importance and a fruitful direction for future research. As the recent differential descriptions for streak and time lines [WT10, WHT12] allow for their fast computation, related approaches to the one described in this paper may become feasible for streak and time surfaces, too.

Acknowledgments

We thank Fritz Kemmler for his help with the user study, and all participants for their time. The CYLINDER data is courtesy of Simone Camarri and co-workers. The MIXER data set is courtesy of Richard Hann, ANSYS Inc. The BÉNARD data set was obtained using the software NaSt3DGP, University of Bonn. Finally, we thank David Coeurjolly from LIRIS, Lyon for his distance transform code.

References

- [BFTW09] BÜRGER K., FERSTL F., THEISEL H., WESTERMANN R.: Interactive streak surface visualization on the GPU. *IEEE TVCG (Proc. Vis)* 15, 6 (2009), 1259–1266. (Cited on page 7)
- [BWF*10] BORN S., WIEBEL A., FRIEDRICH J., SCHEUERMANN G., BARTZ D.: Illustrative stream surfaces. *IEEE TVCG (Proc. Vis)* 16, 6 (2010), 1329–1338. (Cited on page 2)
- [CB11] CANDELARESI S., BRANDENBURG A.: Decay of helical and nonhelical magnetic knots. *Phys. Rev. E* 84, 1 (2011), 16406–16416. (Cited on page 8)
- [CDSB11] CANDELARESI S., DEL SORDO F., BRANDENBURG A.: Decay of trefoil and other magnetic knots. In *Proc. Advances in Plasma Astrophysics* (2011), pp. 461–463. (Cited on page 7)
- [CFM*13] CARNECKY R., FUCHS R., MEHL S., JANG Y., PEIKERT R.: Smart transparency for illustrative visualization of complex flow surfaces. *IEEE TVCG* 19, 5 (2013), 838–851. (Cited on page 2)
- [CGC*12] CAMP D., GARTH C., CHILDS H., PUGMIRE D., JOY K. I.: Parallel stream surface computation for large data sets. In *Proc. LDAV* (2012), pp. 39–47. (Cited on page 2)
- [CH97] CAI W., HENG P.-A.: Principal stream surfaces. In *Proc. IEEE Vis* (1997), pp. 75–81. (Cited on pages 2 and 4)
- [CSBI05] CAMARRI S., SALVETTI M.-V., BUFFONI M., IOLLO A.: Simulation of the three-dimensional flow around a square cylinder between parallel walls at moderate Reynolds numbers. In *AIMETA XVII* (2005). (Cited on page 7)
- [ELC*12] EDMUNDS M., LARAMEE R. S., CHEN G., MAX N., ZHANG E., WARE C.: Surface-based flow visualization. *C&G* 36, 8 (2012), 974–990. (Cited on pages 1 and 2)
- [ELM*12] EDMUNDS M., LARAMEE R. S., MALKI R., MASTERS I., CROFT T. N., CHEN G., ZHANG E.: Automatic stream surface seeding: A feature-centered approach. *CGF (Proc. EuroVis)* 31, 3 (2012), 1095–1104. (Cited on pages 2, 7, and 9)
- [EML*12] EDMUNDS M., MCLOUGHLIN T., LARAMEE R. S., CHEN G., ZHANG E., MAX N.: Advanced, automatic stream surface seeding and filtering. In *Proc. TPCG* (2012), pp. 53–60. (Cited on pages 2, 4, 6, and 7)
- [FCTB08] FABBRI R., COSTA L. D. F., TORELLI J. C., BRUNO O. M.: 2D euclidean distance transform algorithms: A comparative survey. *ACM Comput. Surv.* 40, 1 (2008), 2:1–2:44. (Cited on page 4)
- [GRT13] GÜNTHER T., RÖSSL C., THEISEL H.: Opacity optimization for 3D line fields. *ACM TOG (Proc. SIGGRAPH)* 32, 4 (2013), 120–120. (Cited on pages 6 and 7)
- [GSM*14] GÜNTHER T., SCHULZE M., MARTINEZ ESTURO J., RÖSSL C., THEISEL H.: Opacity optimization for surfaces. *CGF (Proc. EuroVis)* 33, 3 (2014), (to appear). (Cited on pages 2 and 9)
- [HGH*10] HUMMEL M., GARTH C., HAMANN B., HAGEN H., JOY K.: Iris: Illustrative rendering for integral surfaces. *IEEE TVCG (Proc. Vis)* 16, 6 (2010), 1319–1328. (Cited on pages 2, 6, and 9)
- [Hul92] HULTQUIST J. P. M.: Constructing stream surfaces in steady 3D vector fields. In *Proc. IEEE Vis* (1992), pp. 171–178. (Cited on pages 2 and 6)
- [JL97] JOBARD B., LEFER W.: Creating evenly-spaced streamlines of arbitrary density. In *Proc. EG VisSci* (1997), pp. 45–55. (Cited on page 4)
- [KGV83] KIRKPATRICK S., GELATT C. D., VECCHI M. P.: Optimization by simulated annealing. *Science* 220, 4598 (1983), 671–680. (Cited on page 3)
- [KKKW05] KRÜGER J., KIPFER P., KONDRATIEVA P., WESTERMANN R.: A particle system for interactive visualization of 3D flows. *IEEE TVCG* 11, 6 (2005), 744–756. (Cited on page 2)
- [LvWJH04] LARAMEE R. S., VAN WIJK J. J., JOBARD B., HAUSER H.: ISA and IBFVS: Image space based visualization of flow on surfaces. *IEEE TVCG* 10, 6 (2004), 637–648. (Cited on page 2)
- [MLP*10] MCLOUGHLIN T., LARAMEE R. S., PEIKERT R., POST F. H., CHEN M.: Over two decades of integration-based, geometric flow visualization. *CGF* 29, 6 (2010), 1807–1829. (Cited on pages 2 and 9)
- [MSRT13a] MARTINEZ ESTURO J., SCHULZE M., RÖSSL C., THEISEL H.: Global selection of stream surfaces. *CGF (Proc. EG)* 32, 2 (2013), 113–122. (Cited on pages 1, 2, 3, 4, 6, 7, 8, and 9)
- [MSRT13b] MARTINEZ ESTURO J., SCHULZE M., RÖSSL C., THEISEL H.: Poisson-based tools for flow visualization. In *Proc. IEEE PacificVis* (2013), pp. 241–248. (Cited on pages 2 and 7)
- [PS09] PEIKERT R., SADLO F.: Topologically relevant stream surfaces for flow visualization. In *Proc. SCCG* (2009), pp. 43–50. (Cited on page 2)
- [Sab10] SABIN M.: *Analysis and Design of Univariate Subdivision Schemes*. Springer, 2010. (Cited on page 6)
- [SGRT12] SCHULZE M., GERMER T., RÖSSL C., THEISEL H.: Stream surface parametrization by flow-orthogonal front lines. *CGF (Proc. SGP)* 31, 5 (2012), 1725–1734. (Cited on pages 2 and 7)
- [SH95] SUJUDI D., HAIMES R.: *Identification Of Swirling Flow In 3-D Vector Fields*. Tech. rep., MIT, 1995. (Cited on page 9)
- [ST94] SAITO T., TORIWAKI J.-I.: New algorithms for euclidean distance transformation of an n-dimensional digitized picture with applications. *Pattern Recognition* 27, 11 (1994), 1551–1565. (Cited on page 4)
- [SWH05] SAHNER J., WEINKAUF T., HEGE H.-C.: Galilean invariant extraction and iconic representation of vortex core lines. In *Proc. EuroVis* (2005), pp. 151–160. (Cited on page 7)
- [TSW*05] THEISEL H., SAHNER J., WEINKAUF T., HEGE H.-C., SEIDEL H.-P.: Extraction of parallel vector surfaces in 3D time-dependent fields and application to vortex core line tracking. In *Proc. IEEE Vis* (2005), pp. 631–638. (Cited on page 7)
- [TWH03] THEISEL H., WEINKAUF T., HEGE H.-C., SEIDEL H.-P.: Saddle connectors - an approach to visualizing the topological skeleton of complex 3d vector fields. In *Proc. IEEE Vis* (2003), pp. 225–232. (Cited on page 2)
- [vW93] VAN WIJK J. J.: Implicit stream surfaces. In *Proc. IEEE Vis* (1993), pp. 245–252. (Cited on pages 2 and 4)
- [WHT12] WEINKAUF T., HEGE H.-C., THEISEL H.: Advected tangent curves: A general scheme for characteristic curves of flow fields. *CGF (Proc. Eurographics)* 31, 2 (2012), 825–834. (Cited on page 9)
- [WSE05] WEISKOPF D., SCHAFHITZEL T., ERTL T.: Real-time advection and volumetric illumination for the visualization of 3D unsteady flow. In *Proc. EuroVis* (2005), pp. 13–20. (Cited on page 7)
- [WT10] WEINKAUF T., THEISEL H.: Streak lines as tangent curves of a derived vector field. *IEEE TVCG (Proc. Vis)* 16, 6 (2010), 1225–1234. (Cited on page 9)
- [WTH04] WEINKAUF T., THEISEL H., HEGE H.-C., SEIDEL H.-P.: Boundary switch connectors for topological visualization of complex 3D vector fields. In *Proc. VisSym* (2004), pp. 183–192. (Cited on page 2)